Particle Size, Surface Coating, and PEGylation Influence the Biodistribution of Quantum Dots in Living Mice

*Meike L. Schipper, Gopal Iyer, Ai Leen Koh, Zhen Cheng, Yuval Ebenstein, Assaf Aharoni, Shay Keren, Laurent A. Bentolila, Jianquing Li, Jianghong Rao, Xiaoyuan Chen, Uri Banin, Anna M. Wu, Robert Sinclair, Shimon Weiss, and Sanjiv S. Gambhir**

This study evaluates the influence of particle size, PEGylation, and surface coating on the quantitative biodistribution of near-infrared-emitting quantum dots (QDs) in mice. Polymer- or peptide-coated ^{64}Cu-labeled QDs 2 or 12 nm in diameter, with or without polyethylene glycol (PEG) of molecular weight 2000, are studied by serial micropositron emission tomography imaging and region-of-interest analysis, as well as transmission electron microscopy and inductively coupled plasma mass spectrometry. PEGylation and peptide coating slow QD uptake into the organs of the reticuloendothelial system (RES), liver and spleen, by a factor of 6–9 and 2–3, respectively. Small particles are in part renally excreted. Peptide-coated particles are cleared from liver faster than physical decay alone would suggest. Renal excretion of small QDs and slowing of RES clearance by PEGylation or peptide surface coating are encouraging steps toward the use of modified QDs for imaging living subjects.

Keywords:
- biodistribution
- imaging
- nanoparticles
- quantum dots
- tomography

1. Introduction

Quantum dots (QDs) are interesting novel fluorescent semiconductor nanocrystals with potential applications in small-animal imaging in vivo. They have favorable optical properties, including high quantum yield, resistance to photobleaching, narrow emission peak, tunable emission wavelength, and constant excitation profile regardless of

[*] Dr. M. L. Schipper, Prof. Z. Cheng, Dr. S. Keren, Prof. J. Rao, Prof. X. Chen, Prof. S. S. Gambhir
Molecular Imaging Program at Stanford (MIPS)
Departments of Radiology and Bioengineering, Bio-X Program
Stanford University
318 Campus Drive, Palo Alto, CA 94305-5427 (USA)
E-mail: sgambhir@stanford.edu
Dr. G. Iyer, Dr. Y. Ebenstein, Dr. L. A. Bentolila, J. Li, Prof. S. Weiss
California NanoSystems Institute (CNSI) and
Department of Chemistry and Biochemistry
UCLA School of Medicine
Los Angeles, CA 90005-1770 (USA)
A. L. Koh, Prof. R. Sinclair
Stanford Nanocharacterization Laboratory
Department of Materials Science and Engineering
Stanford University
Palo Alto, CA 94305-5427 (USA)
Prof. A. M. Wu
Crump Institute for Molecular Imaging and
Department of Molecular & Medical Pharmacology
UCLA School of Medicine
Los Angeles, CA 90005-1770 (USA)
Prof. A. Aharoni Prof. U. Banin
Department of Physical Chemistry and the
Center for Nanoscience and Nanotechnology
The Hebrew University of Jerusalem
Givat Ram, Jerusalem (Israel)

DOI: 10.1002/smll.200800003

NANO MICRO small

emission wavelength.[1,2] QDs are hydrophobic and have to be solubilized by hydrophilic surface coatings for in vivo applications.[2] Targeting molecules, such as antibodies,[3] aptamers,[4] peptides,[5–7] folate,[8] or high-molecular-weight dextran,[9] can be conjugated to the surface coating. Polyethylene glycol (PEG) increases QD circulation times,[10–13] most likely through sterically hindering the adsorption of opsonizing proteins, which in turn delays recognition and clearance of particles by the reticuloendothelial system (RES).[10,12] Opsonization describes mechanisms of the immune system to make foreign particles (such as bacteria, viruses, or foreign bodies) more recognizable to those cells in the immune system that are involved in fighting them. This usually involves the attachment of proteins (such as activated complement proteins or antibodies) to the foreign agent (such as a QD particle) that then ''flag'' it for the fighting cells (e.g., macrophages).

QDs have recently been used for in vivo fluorescence imaging. Applications include fluorescence sentinel lymph node mapping[14–19] and diffusion analysis of the brain extracellular space.[20] Akerman et al. directed cadmium selenide/zinc sulfide (CdSe/ZnS) QDs, coated with PEG of molecular weight (MW) 5000 and targeting peptides, to lung and tumor vasculature.[5] Our group[6] and others[3] have reported in vivo fluorescence imaging of targets expressed in tumor vasculature and tumor tissues. Our group targeted $\alpha_v\beta_3$ integrin with RGD peptide and MW 2000 PEG-coated CdSe/ZnS QDs.[6] Prostate-specific membrane antigen (PSMA) was targeted with anti-PSMA monoclonal antibodies and 5000 MW PEG-coated CdSe/ZnS QDs.[3] Evidence has been presented of significant QD uptake in liver and spleen,[21] and we have recently presented the first full investigation of temporal and quantitative QD distribution in mice based on positron emission tomography (PET) imaging.[13] Efficient clearance of QDs 12–21 nm in diameter from the bloodstream by the RES was found, with up to 35% of the injected dose per gram of tissue (% ID g^{-1}) taken up by liver, and 12% ID g^{-1} by the spleen. Accumulation was rapid, with 90% of final uptake in these organs reached within 2 min in non-PEGylated QDs, and 6 min in QDs with 2000 MW PEG. Rapid RES clearance of the majority of particles makes it difficult to direct significant amounts of particles to a desired target. While vascular endothelial targets may be reached in vivo, it appears less likely that extravascular targets could be reached, which require longer circulation times because extravasation of the imaging agent is necessary.

A potential way to achieve extravasation despite short circulation times exists in the form of very small indium arsenide (InAs) QDs, which have recently been proposed by us and others.[19,22] Due to the physical properties of bulk InAs, particles emitting in the near-infrared (NIR) window suitable for tissue imaging (700–900 nm) are in the size range of about 1–4 nm. Smaller particles might be able to extravasate more rapidly than larger NIR-emitting QDs. This might be particularly useful when targeting tumors, which tend to have dysfunctional, leaky vessels due to upregulation of neovascularization. Another significant advantage of using smaller-diameter QDs might emerge if their small size results in altered biodistribution patterns, such as renal filtration of the QDs. Biodistribution patterns are of paramount importance in assessing the usefulness of an imaging or therapy agent. Clearance of the agent (e.g., through opsonization by serum proteins and subsequent sequestration by the RES, and/or through kidney filtration) needs to be balanced with the ability to reach the intended target (by crossing natural barriers, such as endothelium, cellular, and nuclear membranes), and bind to it with high affinity. All larger QDs studied to date are quickly taken up by liver, spleen, and, to a minor degree, bone.[6,13,21] It has not been shown that QDs leave these organs once inside, or that they ultimately are cleared from the organism. QD cores are made of toxic materials, such as cadmium, indium, or arsenide. While the core is usually covered by an inert, nontoxic shell which serves to enhance fluorescence and protects the toxic core from degradation, one would prefer to use QDs that are eliminated from the body over time, rather than working with particles that are essentially deposited in organs forever or until broken down.

We have recently presented the first quantitative biodistribution study of QDs in mice. We demonstrated that the uptake of commercially available QDs in liver, spleen, and, to a minor degree, bone is rapid, and that there is no evidence of excretion once particles are taken up by the RES organs. Herein, we investigate whether the use of novel, smaller InAs QD cores, surface coating with amphiphilic peptides, and PEGylation can slow or abate rapid RES uptake and encourage excretion of nanoparticles.

2. Results

2.1. Transmission Electron Microscopy Imaging and Electron-Dispersive Spectroscopy Confirm Renal Excretion of Small InAs QDs

Transmission electron microscopy (TEM) imaging with or without phosphotungstic acid (PTA) counterstaining revealed all QDs to be well dispersed and crystalline, although the InAs cores were not uniform in size (Figure 1). Energy-dispersive spectroscopy (EDS) elemental analysis confirmed the presence of Cd and Se peaks in Qdot800 preparations, as well as a small In peak in the case of InAs QD (data not shown).

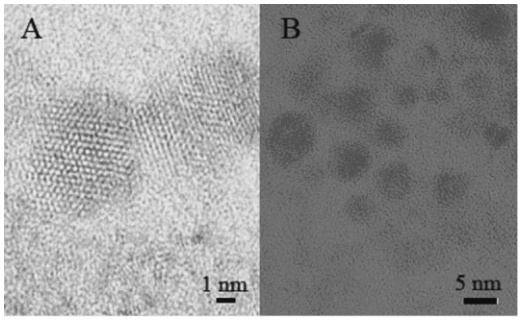

Figure 1. TEM images of A) polymer-coated, PEGylated CdSe QDs and B) peptide-coated, PEGylated InAs QD cores. Samples were imaged on glow-discharged, ultrathin carbon Type A TEM grids using a CM20-FEG microscope operating at 200 kV. TEM imaging revealed all QDs to be well dispersed and crystalline.

2.2. PEGylation with 2000 MW Linear PEG Delays Uptake of Large, Polymer-Coated QDs into Liver and Spleen, and Leads to Low Levels of Bone Uptake

Following tail-vein injection, dynamic imaging revealed a brief peak in heart and lung activity, as expected from a transient increase in blood-pool activity. Liver and spleen were the organs of predominant uptake of QDCpoly (Figure 2, lower panel; Figure 3, first row, left).

Uptake into these organs was rapid. Within 1 min of the appearance of radioactivity in the blood, liver and spleen activity levels were within 1 standard deviation (SD) of their highest values (27.4(±6.1) and 8.1(±7.0)% ID g^{-1} for liver and spleen, respectively). All other organs showed negligible (<2% ID g^{-1}) uptake 10 min after injection and for the remainder of the study. Activity in liver and spleen did not decrease or increase significantly throughout the remainder of the study once physical decay of the radiolabel was accounted for.

As seen with QDCpoly, liver and spleen were the dominant organs of uptake for QDCpolyPEG (33.6(±3.3) and 12.3(±4.0)% ID g^{-1} for liver and spleen, respectively; Figure 2, upper panel; Figure 3, second row, left). However, there were two major differences in biodistribution when compared to QDCpoly. Uptake into liver and spleen was slower, and the time for liver and spleen to be within 1 SD of their respective peak activities was 6 min (as opposed to 1 min for QDCpoly). Second, bone uptake was much higher for QDCpolyPEG than QDCpoly (6.5(±1.2) as compared to 1.7(±0.4)% ID g^{-1}; Figure 2, lower panel). Liver activity remained constant throughout the remainder of the study after accounting for physical decay.

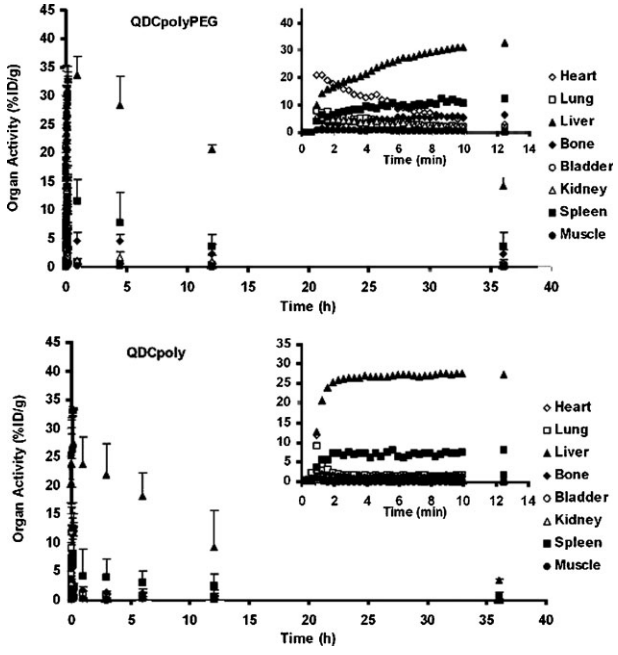

Figure 2. Image-based in vivo biodistribution of ^{64}Cu-labeled, polymer-coated, PEGylated CdSe QDs (QDCpolyPEG, upper panel) and ^{64}Cu-labeled, polymer-coated, unPEGylated CdSe QDs (QDCpoly, lower panel) as measured by image region-of-interest (ROI) analysis of microPET datasets. Radiolabeled QDs (150 μCi) were injected into the tail vein of nude mice ($n = 5$) during dynamic image acquisition. Dynamic imaging was conducted in ten frames of 10 s, followed by ten frames of 20 s, five frames of 60 s, and then 5-min frames over the remainder of the 60 min following injection; 5-min static acquisitions were made at 3, 6, 12, and 36 h after injection. The resulting images were co-registered with microcomputed tomography (microCT) images, and AMIDE image analysis software was used to obtain organ activity information. The mean and SD of % ID g^{-1} have not been corrected for physical decay. The first 10 min of dynamic imaging are shown magnified in the insets. Here, SD bars have been omitted for clarity.

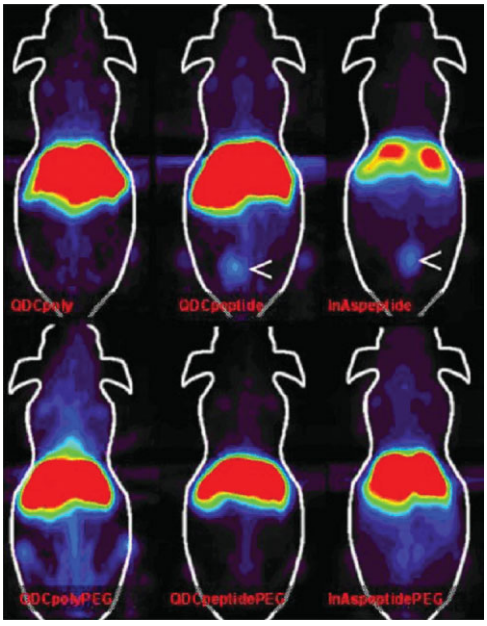

Figure 3. In vivo microPET images of mice injected with ^{64}Cu-labeled, polymer-coated, unPEGylated CdSe QDs (QDCpoly, upper row left), ^{64}Cu-labeled, polymer-coated, PEGylated CdSe QDs (QDCpolyPEG, lower row left), ^{64}Cu-labeled, peptide-coated, unPEGylated CdSe QDs (QDCpeptide, upper row middle), ^{64}Cu-labeled, peptide-coated, PEGylated CdSe QDs (QDCpeptidePEG, lower row middle), ^{64}Cu-labeled, peptide-coated, unPEGylated InAs QDs (InAspeptide, upper row right), and ^{64}Cu-labeled, peptide-coated, PEGylated InAs QDs (InAspeptidePEG, lower row right). The respective imaging agent (150 μCi) was injected into the tail vein of nude mice immediately after starting a 60-min dynamic image acquisition. Coronal maximum intensity projections acquired from 10 to 15 min after injection are shown. Outlines of mice are traced in white for orientation. Bladder uptake in mice treated with QDCpeptide and InAspeptide is indicated by white arrows (<).

2.3. Peptide Coating of Large QDs Prolongs Circulation Time and Leads to Low Levels of Urinary Excretion of UnPEGylated, Peptide-Coated Large QDs

As previously, a brief peak in blood-pool activity was noted in heart and lung after intravenous (i.v.) injection of QDCpeptide, and liver and spleen rapidly took up most of the activity (Figure 4, lower panel; Figure 3, upper row, middle). However, uptake of QDCpeptide into liver and spleen was slightly slower, taking 2 min to reach 1 SD of their highest activity, as opposed to QDCpoly, the polymer-coated QDs (32.3(±4.7) and 4.7(±1.2)% ID g^{-1} for QDCpeptide in liver

NANO MICRO small

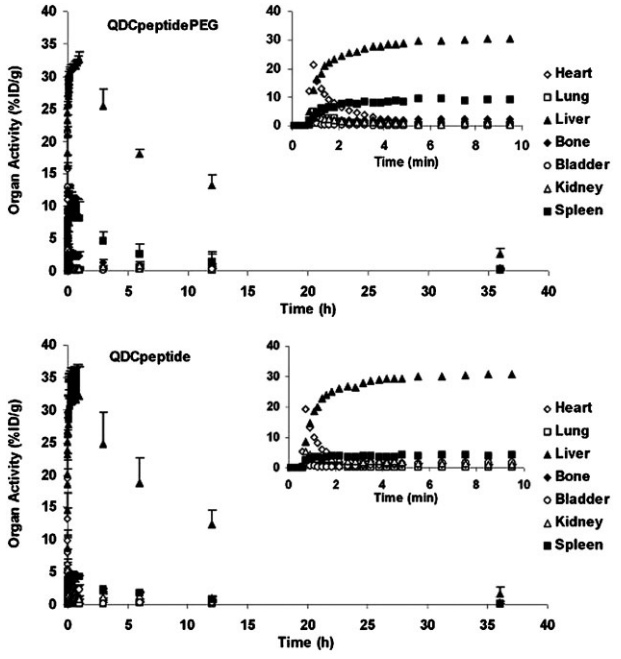

Figure 4. Image-based in vivo biodistribution of ^{64}Cu-labeled, peptide-coated, PEGylated CdSe QDs (QDCpeptidePEG, upper panel) and ^{64}Cu-labeled, peptide-coated, unPEGylated CdSe QDs (QDCpeptide, lower panel) as measured by image ROI analysis of microPET datasets. Radiolabeled QDs (150 μCi) were injected into the tail vein of nude mice ($n = 5$) during dynamic image acquisition. Dynamic imaging was conducted in ten frames of 10 s, followed by ten frames of 20 s, five frames of 60 s, and then 5-min frames over the remainder of the 60 min following injection; 5-min static acquisitions were made at 3, 6, 12, and 36 h after injection. The resulting images were co-registered with microCT images, and AMIDE image analysis software was used to obtain organ activity information. The mean and SD of % ID g^{-1} have not been corrected for physical decay. The first 10 min of dynamic imaging are shown magnified in the insets. Here, SD bars have been omitted for clarity.

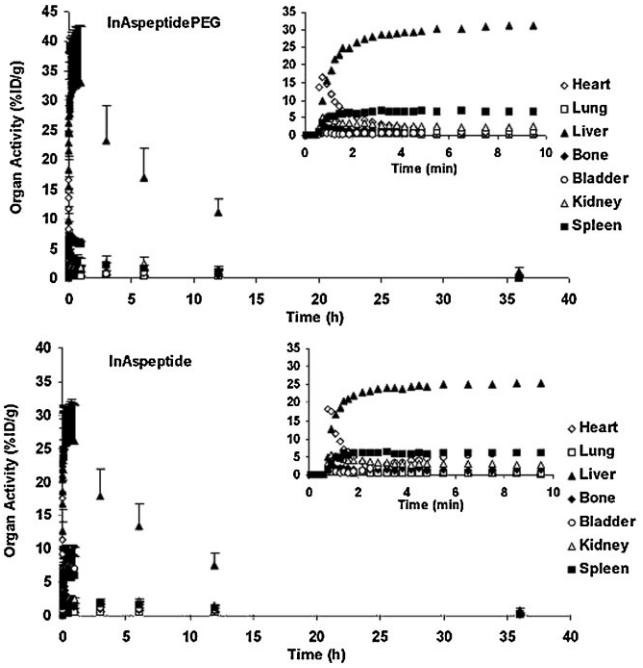

Figure 5. Image-based in vivo biodistribution of ^{64}Cu-labeled, peptide-coated, PEGylated InAs QD cores (InAspeptidePEG, upper panel) and ^{64}Cu-labeled, peptide-coated, unPEGylated InAs QD cores (InAspeptide, lower panel) as measured by image ROI analysis of microPET datasets. Radiolabeled QDs (150 μCi) were injected into the tail vein of nude mice ($n = 5$) during dynamic image acquisition. Dynamic imaging was conducted in ten frames of 10 s, followed by ten frames of 20 s, five frames of 60 s, and then 5-min frames over the remainder of the 60 min following injection; 5-min static acquisitions were made at 3, 6, 12, and 36 h after injection. The resulting images were co-registered with microCT images, and AMIDE image analysis software was used to obtain organ activity information. The mean and SD of % ID g^{-1} have not been corrected for physical decay. The first 10 min of dynamic imaging are shown magnified in the insets. Here, SD bars have been omitted for clarity.

and spleen; Figure 2, lower panel). Interestingly, a small but significant amount of activity was seen in the bladder (2.5(±0.1)% ID g^{-1} for QDCpeptide as opposed to 0.1(±0.0)% ID g^{-1} for QDCpoly). Again, uptake in all other organs was negligible (<2% ID g^{-1}) 10 min after injection and for the remainder of the study. Organ activity decreased faster than would be expected from physical decay of copper alone, reaching levels of statistical significance at 12 h in liver ($p < 0.02$).

As noted in QDCpolyPEG, QDCpeptidePEG was taken up into liver and spleen (32.4(±1.2) and 9.4(±3.9)% ID g^{-1} for liver and spleen, respectively; Figure 4, upper panel; Figure 3, lower row, middle) more slowly than its unPEGylated counterpart, QDCpeptide. In addition, QDCpeptidePEG uptake into liver and spleen was also slower than seen with QDCpolyPEG. One SD of peak liver activity of QDCpeptidePEG was reached after 19 min had elapsed, as opposed to 6 SD for QDCpolyPEG. Once again, some bone uptake was noted (2.4(±0.3) for QDCpeptidePEG as compared to 1.2(±0.1)% ID g^{-1} for QDCpeptide). In contrast to QDCpeptide, bladder uptake of QDCpeptidePEG was not significant (0.4(±0.1)% ID g^{-1}). As seen previously for QDCpeptide, liver activity of QDCpeptidePEG decreased faster than expected from physical decay alone ($p < 0.05$ for liver at 3 h).

2.4. Small, Peptide-Coated InAs QDs Are Excreted through the Kidney, but Liver and Spleen Clear the Majority of the Injected Activity

Following a brief blood-pool activity peak in heart and lung, liver and spleen rapidly took up most of the injected activity of InAspeptide (Figure 5, lower panel; Figure 3, upper row, right) within a time frame similar to QDCpeptide (26.6(±5.7) and 6.2(±3.7)% ID g^{-1} for liver and spleen; 2 min to reach 1 SD of highest activity). Although kidney uptake was not significantly different from that for QDCpeptide (maximum 5.5(±1.0)% ID g^{-1} at 55 s for InAspeptide versus 5.4(±0.8)% ID g^{-1} at 45 s for QDCpeptide), the bladder activity of InAspeptide was markedly higher (7.6(±3.6)% ID g^{-1} for InAspeptide as opposed to 2.5(±0.1)% ID g^{-1} for QDCpeptide). All other organs had uptake levels < 2% ID g^{-1}. Once again, InAspeptide activity was cleared from liver

more quickly than expected from physical decay alone ($p < 0.05$ at 6 h).

InAspeptidePEG was also accumulated by liver and spleen (33.2(±9.6) and 7.0(±3.0)% ID g^{-1}; Figure 5, upper panel; Figure 3, lower row, right). However, these PEGylated particles were accumulated as swiftly as their unPEGylated counterparts InAspeptide (2 min to 1 SD of maximum liver activity for both InAspeptidePEG and InAspeptide). Unlike other PEGylated compounds, only low amounts of InAspeptidePEG were taken up into bone (1.5(±0.4)% ID g^{-1}). Bladder uptake of InAspeptidePEG was low, but higher than that of its larger counterpart, QDCpeptidePEG (1.5(±0.4)% ID g^{-1} versus 0.4(±0.1)% ID g^{-1}). Like InAspeptide, InAspeptidePEG activity in the liver had a significantly shorter half-life than that expected from physical decay alone ($p < 0.05$ at 12 h). Inductively coupled plasma mass spectrometry (ICP-MS) analysis of mouse urine demonstrated 11.02 ng mL^{-1} (9.6 nM; relative standard deviation, %RSD = 2.39) of indium and 4.778 ng mL^{-1} (6.45 nM; %RSD = 1.79) of arsenide. The In:As ratio was 1.48:1, compared to undetectable levels of these elements in control urine.

Clinical observation did not reveal any signs of toxicity following injection of any of the compounds tested here over at least 72 h, including unusual behavior, such as vocalizations, labored breathing, difficulties moving, hunching, or unusual interactions with cagemates.

3. Discussion

QDs are promising novel agents for biomedical applications in vivo. To assess their usefulness, it is important to characterize their behavior in living animals, rather than rely on ex vivo measurements and theoretical considerations alone. Due to tissue absorption of light, QD biodistribution in living animals cannot be quantified accurately from fluorescence measurements. Preliminary studies from our laboratory show that fluorescence imaging systems significantly underestimate QD mass amounts in living animals, especially when located in deeper-lying tissues, and are currently not robust enough for biodistribution purposes (data not shown). In contrast, PET scanning accurately measures radioactivity in three-dimensional systems.[23] We used microPET-based imaging of radiolabeled QDs and quantitative image analysis software to investigate the influence of size, surface coating, and PEGylation on the quantitative biodistribution of QDs in living mice.

As shown in our previous work,[13] most QD formulations are cleared from the circulation within a relatively short time (20 min) by liver and spleen, the primary organs of the RES. Depending on the physicochemical properties of the QDs, plausible mechanisms of interactions of QDs with biological tissues have been presented.[24,25] The accumulation of PEGylated QDs in the liver, spleen, and, to a marginal extent, in other organs observed here explains some of the observations described by Maysinger et al.[24] and Nel et al.,[25] such as particle dissolution or electrostatic, hydrophobic, and hydrophilic interactions with its intracellular environment. In addition, incomplete passivation of the QD surface may lead to active electronic configurations resulting in electron donor–acceptor interactions with macromolecules present in the intracellular milieu of the mouse.

The accumulation and redistribution of PEGylated QDs (polymer- or peptide-coated) led us to explore the potential of small InAs cores to evade the RES. The specific QD preparation used in this study consists of the smallest InAs QD available to us at the time of the experiment. Due to their low fluorescence quantum yield (<1%), they are not suitable for fluorescence imaging. Rather, they serve as model carriers of the radiolabel, which enable assessment of small QD biodistribution. Recent synthetic efforts indicate that bright NIR particles with equivalent size may be synthesized.[19] Such QDs will be the focus of future studies. Interestingly, small InAs QDs did not follow the pattern observed in larger QDs, and PEGylated particles were taken up into liver as swiftly as their non-PEGylated counterparts. Recent results by Choi et al. suggest a size threshold of 5.5 nm for glomerular filtration of neutrally charged or zwitterionic QDs, and that PEGylation of QDs results in a total hydrodynamic diameter above this cutoff level.[26] Although our particles meet this criterion under ex vivo conditions, it is possible that the hydrodynamic radius is significantly increased in vivo.

As shown for many other nanoparticles,[10–12] QDs are likely to be opsonized by serum proteins, such as clotting and complement proteins, which "tag" them for RES clearance. Accordingly, surface modification with 2000 MW linear PEG, which has been shown to protect nanoparticles from opsonization,[10–12] increased the blood circulation time of large QD particles six- to ninefold to a maximum of 18 min. Circulation times observed by us did not reach those reported previously for QDs coated with 5000 MW PEG (up to 140 min, as measured by fluorescence imaging).[14,21] This is in part attributable to differences in measuring methodology. In this study, the time point at which liver was within 1 SD of its maximal activity was chosen as a quantitative cutoff point, whereas in Reference [21] measurement continued as long as any fluorescence signal could be detected in blood.

Also, the circulation half-life of nanoparticles varies depending on a range of factors, and does not increase linearly with PEG chain length.[10] Circulation half-life may be influenced by changes in PEG tertiary structure, PEG density, the surface potential of the underlying nanostructure,[10–12] and the amount of nanoparticles injected. At doses below 20 nmol kg^{-1}, 2000 MW PEG-coated liposomes will be cleared rapidly from blood. This is attributed to a pool of preexisting opsonic factors, which is depleted as higher doses are given.[27–29] In the study presented here, doses of 0.8–1.25 nmol kg^{-1} QDs were administered. As previously observed by our group,[13] bone uptake coincided with increased serum circulation times, as secondary RES locations, such as macrophages in bone marrow, participated in the clearance process.

Surface coating with peptides instead of polymer prolonged the serum half-life of QD particles two- to threefold. This effect was observed when both unPEGylated and PEGylated large QD particles were compared. As the polymer coating is proprietary to the manufacturer, we were unable to construct polymer-coated InAs particles and cannot

NANO MICRO small

make assumptions as to whether this is also true for small InAs particles. As mentioned above, the surface charge of the underlying nanoparticle is an important factor which may influence circulation times.[10–12] In this case, it most likely mediates a decreased affinity of the peptide coating to opsonizing proteins, when compared to the polymer. Further study will help to fully elucidate the mechanism.

Evidence suggests that the smallest peptide-coated particles studied here are excreted through the kidneys. The presence of peptide-coated QD cores in urine was determined by ICP-MS, which has previously been used to quantify the elemental composition of QDs.[30,31] Fischer et al.[32] have evaluated the presence of cadmium in blood and tissues by using ICP atomic emission spectroscopy (ICP-AES) from mice intravenously injected with organic acid and bovine serum albumin-coated QDs. The absence of indium and arsenide in urine from mice that had not been injected with QD cores suggests that ICP-MS could be adapted for the quantification of InAs cores. In this study, we provide evidence for the first time of the presence of indium and arsenide, the elements in the cores of the QDs, by ICP-MS analysis of mouse urine. Bladder activity in a biodistribution study is strongly suggestive of renal excretion. Even so, it is by itself not an unambiguous finding and could be caused by free radiolabel, or radiolabeled degradation products, rather than by the excreted nanoparticle. However, the presence of indium and arsenide in the urine of mice injected with InAspeptide as measured by ICP-MS proves that the small InAs QDs used here are indeed being excreted renally. Our findings are consistent with recent results by Choi et al., who showed that zwitterionic or neutrally charged QDs below a diameter of 5.5 nm are renally excreted.[26]

The presence of renally excreted QDs is encouraging for two reasons. Firstly, it simply confirms that the QDs used here have a hydrodynamic radius below 5.5 nm, small enough to be filtered through the glomeruli. The smaller the hydrodynamic radius of a particle, the more likely it is that it will be able to cross the vascular endothelial basement membrane of blood vessels, which is a prerequisite for reaching targets that are expressed in tissues, rather than on the vascular endothelium. Stroh et al. have found no extravasation of larger CdSe QDs from tumor vessels (which are rather more ''leaky'' than normal vessels) using intravital microscopy.[9] Although the smaller QDs used in our study do not escape recognition and clearance by the RES per se, they might be able to extravasate from vessels quickly enough to be able to reach tumor or interstitial targets in relevant amounts.

The second reason that renal filtration of small peptide-coated InAs QDs is encouraging is that it simply represents a way for them to leave the body. The fate of QDs accumulated in the liver and spleen has not been studied, but the RES is likely to either break down QDs or store them indefinitely. Although no toxicity was observed by us clinically for at least 72 h after injection, and no reports of in vivo toxicity of QDs exist, it is not known whether toxicity might be caused by the long-term presence of residual QDs in the liver and spleen, and studies that will address this question are an important future field of research.

Interestingly, the activity of peptide-coated QDs in liver decreased significantly faster than might be expected from physical decay of the radiolabel, whereas the activity of polymer-coated QDs did not. This might be caused either by breakdown of peptide-coated particles and excretion of the radiolabel with or without the chelator and parts of the peptide coating, or it might signify recirculation of peptide-coated QDs and subsequent excretion, likely through the kidney. At present, the fate of QDs upon entering the liver and spleen is poorly understood, and we are actively pursuing research in this area.

Any agent used for imaging should fulfill three criteria to achieve a high target-to-background ratio: it should quickly reach the site of the target, bind to it with high specificity and affinity, and unbound agent should be effectively cleared to reduce background ''noise''. We observe relatively swift RES clearance of QDs from the circulation, which allows little time to reach potential targets. However, the circulation time can be increased through the use of an improved peptide surface coating and PEGylation, and renal excretion of small particles raises hopes that transport through vascular endothelium might be achieved. The findings presented herein are encouraging steps toward making QDs useful in vivo imaging agents.

In contrast to a recent report assaying organ distribution of small QDs at a single time point (4 h after injection[26]), our study provides complete quantitative biodistribution information over time, with the possibility to directly assess organ exposure to QDs by measuring the area under the time activity curve of the respective organ. This provides a more complete understanding of the in vivo behavior of QDs, which cannot be simply inferred from ex vivo characterizations, but rather has to be investigated in the living animal for each new nanoparticle.

In summary, this work investigates the influence of particle size, surface coating, and PEGylation on the biodistribution of QDs in living mice. While overall circulation times were relatively short, and the majority of QDs were cleared by liver and spleen, blood half-life could be prolonged by a factor of 2–3 through peptide coating of particles, and by a factor of 6–9 through PEGylation with 2000 MW linear PEG. Small InAs cores were renally excreted in part, which is an encouraging step toward generating probes that are able to access extravascular targets and are ultimately cleared from the organism. The use of smaller-diameter particles and surface passivation is critical for adopting QDs as in vivo imaging agents.

4. Conclusions

PEGylation and peptide coating slow QD uptake by the RES by factors of 6–9 and 2–3, respectively. Small InAs particles are in part renally excreted. Renal excretion of small InAs QDs and slowing of RES clearance by PEGylation or peptide surface coating are encouraging steps toward the use of modified QDs for imaging living subjects.

Table 1. Peptides used for solubilization and conjugation of PEG-2000 and ^{64}Cu to QDs.

Acronym	Peptide sequence
sKFC3	NH_2-Lys-Gly-Ser-Glu-Ser-Gly-Gly-Ser-Glu-Ser-Gly-Phe-Cys-Cys-Phe-Cys-Cys-Phe-Cys-Cys-Phe-$CONH_2$
sDFC3	DOTA-Gly-Leu-Gly-Gly-Glu-Ser-Gly-Gly-Ser-Glu-Ser-Gly-Phe-Cys-Cys-Phe-Cys-Cys-Phe-Cys-Cys-Phe-$CONH_2$

5. Experimental Section

QDs: Six QD conjugations were used: Qdot800 ITK amino (PEG) (''QDCpolyPEG''), and Qdot800 ITK carboxyl (''QDCpoly'') core–shell QDs were purchased from Invitrogen (Carlsbad, CA). They were coated with a proprietary polymer to render them water soluble, which was covalently conjugated with 2000 MW PEG, where applicable. The reported diameter of these particles is 21 and 19 nm for PEGylated and unPEGylated particles, respectively (Invitrogen). For ''QDCpeptidePEG'' and ''QDCpeptide'', uncoated core–shell nanocrystals (Invitrogen) were rendered water soluble by coating with a peptide monolayer, and then were covalently conjugated with 2000 MW PEG, where applicable, as described previously.[33] These particles have a core diameter of 10 nm for both the PEGylated and unPEGylated particles, which corresponds to 12 and 11 nm for the complete unPEGylated and PEGylated particles. ''InAspeptidePEG'' and ''InAspeptide'' were prepared from InAs core nanocrystals synthesized as previously described.[22] TEM images as well as a broad emission peak centered at 825 nm indicated a core diameter of about 2($\pm$1) nm. Dynamic light scattering measurements of the peptide-coated particles in phosphate-buffered saline (PBS) indicated a final hydrodynamic radius of about 5($\pm$2) nm.

Surface passivation of QDs using peptides: Trioctylphosphine oxide (TOPO)-activated InAs cores were synthesized as described previously.[22] Peptide exchange of QDs was carried out as previously described.[7,33] The peptide sequence is described in Table 1.

Briefly, TOPO-coated QDs (1 μM) were resuspended in pyridine (450 μL) to a concentration of 1 μM. sKFC3 and sDFC3 peptides (4 mg) were dissolved in DMSO (50 μL) and mixed with the QD suspension with concomitant addition of tetramethylammonium hydroxide (≈12 μL) 25% (w/v) in methanol. The resulting mixture was spun at 12 000 rpm for 3 min. The supernatant was decanted and the pellet of peptide-coated QDs was resuspended in DMSO (300 μL). A Sephadex G-25 (Amersham) column was equilibrated with milli-Q water. The peptide-coated QDs (300 μL) were eluted from the column by monitoring the dark brown shadow contributed by the InAs cores. Fractions containing peptide-coated InAs cores were treated with dithiothreitol (1 mM) to remove residual free peptide, and buffer exchange was carried out into PBS (pH 7.2) using a 3K MW-cutoff spin column (Millipore). For the control experiment, peptide sKFC3 was treated as above without the QDs, and fractions were pooled by monitoring the absorbance at 214 and 254 nm. For commercial QDs (Invitrogen Corporation), an isopropanol/methanol mixture (1:3) was used to reflux the QDs at 60 °C. Following centrifugation at 8000 rpm for 2–3 min, peptide exchange was carried out as described above.[7,33] Covalent conjugation of NHS-PEG-2000 (1 mM; NOF Corporation, Japan) to the terminal amine group of sKFC3-conjugated commercial QDs was carried out at pH 8.0 (50 mM borate buffer, 100 mM NaCl) for 3 h, and terminated with Tris buffer (pH 8.0, 50 mM).

Chemistry and radiochemistry: Chemicals were obtained from Sigma–Aldrich Chemical Co. (St. Louis, MO) unless otherwise mentioned. A CRC-15R PET dose calibrator (Capintec Inc., Ramsey, NJ) was used for all radioactivity measurements. For radiolabeling of PEGylated QDs, 1,4,7,10-tetraazacyclododecane-*N*,*N*′,*N*″,*N*‴-tetraacetic acid (DOTA; Macrocyclics Inc., Richardson, TX), 1-ethyl-3-[3-(dimethylamino)propyl]carbodiimide (EDC), and *N*-hydroxysulfonosuccinimide (SNHS) at a molar ratio of 1:1:0.8 were mixed and incubated at 4 °C for 30 min (pH 5.5). PEG-QDs (8.2 μM, 100 μL) were then added to the in situ prepared sulfosuccinimidyl ester of DOTA (DOTA-OSSu) in a theoretical stoichiometry of 1:1000 in sodium borate buffer (50 mM, pH 8.4), mixed, and reacted at 4 °C overnight. The resulting DOTA–PEG–QD conjugate was purified by removing small molecules (MW $<$10 K) by centrifugal filtration (10 K Nanosep). DOTA-labeled QDs (20 μL, 4.1 μM) were radiolabeled with ^{64}Cu (purchased from University of Wisconsin–Madison, Madison, WI) by addition of $^{64}CuCl_2$ (44.4 MBq, 1.2 mCi) in NaOAc (0.1 N, pH 5.5) buffer followed by incubation for 1 h at 37 °C. The radiolabeled complex was purified by centrifugal filtration (10 K Nanosep) and reconstituted in PBS. The radiolabeling yield was usually greater than 95%, and the specific activity was estimated to be above 1 Ci μmol^{-1} for both radiolabeled complexes. This is equivalent to one ^{64}Cu-labeled QD in 100 QDs. Administration of unlabeled QDs was considered to be of advantage, since it allowed us to administer 150 μCi in 25 pmol QDs per animal. We commonly use this QD dose for fluorescence imaging (unpublished observations).

TEM specimen preparation and imaging of QDs: QDCpolyPEG or QDCpoly suspension (5 μL) was pipetted onto an ultrathin carbon Type A TEM grid (Ted Pella Inc., Redding, CA) that had been glow-discharged. After 5 min, the grids were rinsed with deionized water to remove any buffer salts from the sample and wicked to almost dryness with filter paper. For negative staining, PTA (pH 7.0) was then added to the grid and completely dried after 1 min by using filter paper. InAspeptidePEG and InAspeptide were applied to the grids in their native medium, without rinsing. Samples were also obtained from the pooled urine of mice injected with InAs QDs, and from mouse urine spiked with InAs QDs. All TEM analyses were performed at the Stanford Nanocharacterization Laboratory using a CM20-FEG microscope (Philips, Andover, MA) operating at 200 kV. The microscope was equipped with an energy-dispersive X-Ray spectrometer, which allowed compositional identification of the elements present in each sample.

MicroPET imaging: All animal experiments were approved by the Stanford Administrative Panels on Laboratory Animal Care (APLAC). Nude mice were imaged under anesthesia with 2% isoflurane in 2 L min^{-1} of oxygen on a MicroPET R4 scanner (Concorde Microsystems, Knoxville, TN). Dynamic imaging was

NANO MICRO small

initiated immediately prior to tail-vein injection of ^{64}Cu-labeled (150 μCi) QDCpolyPEG, QDCpoly, QDCpeptidePEG, QDCpeptide, InAspeptidePEG, or InAspeptide. This corresponded to approximately 1 pmol g^{-1} animal, tenfold lower than in a recent publication by Choi et al.[26] Dynamic imaging was conducted in ten frames of 10 s, followed by ten frames of 20 s, five frames of 60 s, and then 5-min frames over the remainder of the 60 min following injection. Animals were reimaged at 3, 6, 12, and 36 h after injection using 5-min static acquisitions. Images were reconstructed with an OSEM algorithm. The final image spatial resolution wais 1.66–1.85 mm^3.[23]

MicroCT imaging: Immediately following microPET imaging, nude mice were imaged under anesthesia with 2% isoflurane in 2 L min^{-1} of oxygen on an X-O MicroCT System (Gamma Medica, Northridge, CA). Animals were imaged for 6 min in one bed position. Acquisition parameters were as follows: 75 kVp beam energy, current 210 μA, and 256 projections in a 9.7-cm (*z* axis) field of view. COBRA and AMIDE software was used for image reconstruction and viewing. The spatial resolution of the images was isotropic at 43 μm.

Image-based in vivo biodistribution: For image-based in vivo biodistribution studies of individual animals, reconstructed images were loaded into AMIDE, a free image analysis software package developed in our laboratories.[34] CT and microPET datasets from different time points belonging to each individual animal were first manually aligned to ensure optimal overlap of organs of interest. To obtain time–activity curves, three-dimensional ROIs were then placed over the organs of interest, using both morphologic information from the CT image and functional information from PET images for orientation. Activity per voxel was converted to percent of injected activity per gram of tissue (% ID g^{-1}) using conversion factors obtained by scanning a cylinder phantom filled with a known activity of ^{64}Cu to account for microPET scanner efficiency.[35] The % ID g^{-1} of each organ for the mid point of each frame or time point was then plotted over time.

ICP-MS: Under general anesthesia with 2% isoflurane in 2 L min^{-1} of oxygen, mice were i.v. injected with InAspeptide (150 μL, 1.82 pM μL^{-1}) and kept on a warming pad for 60 min. Urine samples were then collected by manual expression and stored at −80 °C until analysis. Metal analysis was performed at the Elemental Analysis and Speciation Facility at UCLA, Molecular Instrumentation Center, using an Agilent 7500ce ICP mass spectrometer. The spectrometer was equipped with an octapole reaction system for plasma- and matrix-based interference removal. Helium was utilized as collisional gas for polyatomic interference ($ArCl^+$) removal on *m*/*z* 75 (As-75). Indium, monitored at *m*/*z* 115, was analyzed in the no-gas mode. Prior to analysis, Optima-grade nitric acid (100 μL; ThermoFisher Scientific, CA) was added to the urine sample (in a 1.5-mL perfluoroalkoxy conical vial) and allowed to digest at 90 °C in a MOD-Block open-vessel digester (CPI International, CA). After complete digestion, the sample was diluted with 18 MΩ deionized water to achieve a final concentration of 2% HNO_3. A multielement standard (100 ppm; CPI International, CA) was used to generate 1, 10, 100, and 200 ppb (parts per billion) external standard solutions. The ICP-MS analysis parameters were as follows: forward power 1500 W, carrier gas 1.05 L min^{-1}, nebulizer pump 0.12 rps, sample depth 7 mm, helium flow at 4 mL min^{-1}. Three readings were taken per mass and the average reported.

Statistical calculations: Averages, SDs, and the statistical significance of differences between groups (*t*-test) were determined using standard software (Microsoft Excel 2000, Microsoft Corporation, Redmont, WA); p values <0.05 were considered statistically significant.

Acknowledgements

We thank Dr. J. S. T. Ng, Dr. A. M. Lutz, Dr. J. K. Willmann, and Dr. A. M. Loening for helpful discussions. This study was supported in part by NCI ICMIC P50 CA114747 (S.S.G.), NCI U54 (S.S.G.), and NIBIB BRP (S.W.).

[1] X. Gao, L. Yang, J. A. Petros, F. F. Marshall, J. W. Simons, S. Nie, *Curr. Opin. Biotechnol.* **2005**, *16*, 63–72.
[2] X. Michalet, F. F. Pinaud, L. A. Bentolila, J. M. Tsay, S. Doose, J. J. Li, G. Sundaresan, A. M. Wu, S. S. Gambhir, S. Weiss, *Science.* **2005**, *307*, 538–544.
[3] X. Gao, Y. Cui, R. M. Levenson, L. W. Chung, S. Nie, *Nat. Biotechnol.* **2004**, *22*, 969–976. Epub 2004 Jul 2018.
[4] T. C. Chu, F. Shieh, L. A. Lavery, M. Levy, R. Richards-Kortum, B. A. Korgel, A. D. Ellington, *Biosens. Bioelectron.* **2006**, *21*, 1859–1866. Epub 2006 Feb 1821.
[5] M. E. Akerman, W. C. Chan, P. Laakkonen, S. N. Bhatia, E. Ruoslahti, *Proc. Natl. Acad. Sci. USA* **2002**, *99*, 12617–12621. Epub 2002 Sep 12616.
[6] W. Cai, D. W. Shin, K. Chen, O. Gheysens, Q. Cao, S. X. Wang, S. S. Gambhir, X. Chen, *Nano Lett.* **2006**, *6*, 669–676.
[7] F. Pinaud, D. King, H. P. Moore, S. Weiss, *J. Am. Chem. Soc.* **2004**, *126*, 6115–6123.
[8] D. J. Bharali, D. W. Lucey, H. Jayakumar, H. E. Pudavar, P. N. Prasad, *J. Am. Chem. Soc.* **2005**, *127*, 11364–11371.
[9] M. Stroh, J. P. Zimmer, D. G. Duda, T. S. Levchenko, K. S. Cohen, E. B. Brown, D. T. Scadden, V. P. Torchilin, M. G. Bawendi, D. Fukumura, R. K. Jain, *Nat. Med.* **2005**, *11*, 678–682. Epub 2005 May 2008.
[10] C. Allen, N. Dos Santos, R. Gallagher, G. N. Chiu, Y. Shu, W. M. Li, S. A. Johnstone, A. S. Janoff, L. D. Mayer, M. S. Webb, M. B. Bally, *Biosci. Rep.* **2002**, *22*, 225–250.
[11] S. M. Moghimi, J. Szebeni, *Prog. Lipid Res.* **2003**, *42*, 463–478.
[12] D. E. Owens III, N. A. Peppas, *Int. J. Pharm.* **2006**, *307*, 93–102. Epub 2005 Nov 2021.
[13] M. L. Schipper, Z. Cheng, S. W. Lee, L. A. Bentolila, G. Iyer, J. Rao, X. Chen, A. M. Wu, S. Weiss, S. S. Gambhir, *J. Nucl. Med.* **2007**, *48*, 1511–1518.
[14] B. Ballou, L. A. Ernst, S. Andreko, T. Harper, J. A. J. Fitzpatrick, A. S. Waggoner, M. P. Bruchez, *Bioconjugate Chem.* **2007**, *18*, 389–396.
[15] S. W. Kim, J. P. Zimmer, S. Ohnishi, J. B. Tracy, J. V. Frangioni, M. G. Bawendi, *J. Am. Chem. Soc.* **2005**, *127*, 10526–10532.
[16] D. W. Knapp, L. G. Adams, A. M. DeGrand, J. D. Niles, J. A. Ramos-Vara, A. B. Weil, M. A. O'Donnell, M. D. Lucroy, J. V. Frangioni, *Eur. Urol.*, in press.
[17] C. P. Parungo, S. Ohnishi, S. W. Kim, S. Kim, R. G. Laurence, E. G. Soltesz, F. Y. Chen, Y. L. Colson, L. H. Cohn, M. G. Bawendi, J. V. Frangioni, *J. Thorac. Cardiovasc. Surg.* **2005**, *129*, 844–850.

[18] E. G. Soltesz, S. Kim, S. W. Kim, R. G. Laurence, A. M. De Grand, C. P. Parungo, L. H. Cohn, M. G. Bawendi, J. V. Frangioni, *Ann. Surg. Oncol.* **2006**, *13*, 386–396. Epub 2006 Jan 2031.
[19] J. P. Zimmer, S. W. Kim, S. Ohnishi, E. Tanaka, J. V. Frangioni, M. G. Bawendi, *J. Am. Chem. Soc.* **2006**, *128*, 2526–2527.
[20] R. G. Thorne, C. Nicholson, *Proc. Natl. Acad. Sci. USA* **2006**, *103*, 5567–5572. Epub 2006 Mar 5527.
[21] B. Ballou, B. C. Lagerholm, L. A. Ernst, M. P. Bruchez, A. S. Waggoner, *Bioconjugate Chem.* **2004**, *15*, 79–86.
[22] A. Aharoni, T. Mokari, I. Popov, U. Banin, *J. Am. Chem. Soc.* **2006**, *128*, 257–264.
[23] C. Knoess, S. Siegel, A. Smith, D. Newport, N. Richerzhagen, A. Winkeler, A. Jacobs, R. N. Goble, R. Graf, K. Wienhard, W. D. Heiss, *Eur. J. Nucl. Med. Mol. Imaging* **2003**, *30*, 737–747. Epub 2003 Jan 2021.
[24] D. Maysinger, J. Lovric, A. Eisenberg, R. Savic, *Eur. J. Pharm. Biopharm.* **2007**, *65*, 270–281.
[25] A. Nel, T. Xia, L. Madler, N. Li, *Science* **2006**, *311*, 622–627.
[26] H. S. Choi, W. Liu, P. Misra, E. Tanaka, J. P. Zimmer, B. I. Ipe, M. G. Bawendi, J. V. Frangioni, *Nat. Biotechnol.* **2007**, *25*, 1165–1170.
[27] P. Laverman, O. C. Boerman, W. J. G. Oyen, F. H. M. Corstens, G. Storm, *Crit. Rev. Ther. Drug Carrier Syst.* **2001**, *18*, 551–566.
[28] P. Laverman, A. H. Brouwers, E. T. Dams, W. J. Oyen, G. Storm, N. van Rooijen, F. H. Corstens, O. C. Boerman, *J. Pharmacol. Exp. Ther.* **2000**, *293*, 996–1001.
[29] P. Laverman, M. G. Carstens, O. C. Boerman, E. T. Dams, W. J. Oyen, N. van Rooijen, F. H. Corstens, G. Storm, *J. Pharmacol. Exp. Ther.* **2001**, *298*, 607–612.
[30] N. V. Gopee, D. W. Roberts, P. Webb, C. R. Cozart, P. H. Siitonen, A. R. Warbritton, W. W. Yu, V. L. Colvin, N. J. Walker, P. C. Howard, *Toxicol. Sci.* **2007**, *98*, 249–257.
[31] P. Yu, M. C. Beard, R. J. Ellingson, S. Ferrere, C. Curtis, J. Drexler, F. Luiszer, A. J. Nozik, *J. Phys. Chem. B* **2005**, *109*, 7084–7087.
[32] H. C. Fischer, L. Liu, W. Pang, C. W. Chan, *Adv. Funct. Mater.* **2006**, *16*, 1299–1305.
[33] G. Iyer, F. Pinaud, J. Tsay, S. Weiss, *Small* **2007**, *3*, 793–798.
[34] A. M. Loening, S. S. Gambhir, *Mol. Imaging* **2003**, *2*, 131–137.
[35] D. C. Comsa, T. J. Farrell, M. S. Patterson, *Phys. Med. Biol.* **2006**, *51*, 3733–3746. Epub 2006 Jul 3712.

Received: January 1, 2008
Revised: September 16, 2008
Published online: December 2, 2008

